Topology Optimization Under Stress Relaxation Effect Using Internal Element Connectivity Parameterization

Meisam Takalloozadeh
Engineering Department,
Shiraz University,
Zand Blvd., Shiraz 7134851156, Iran
e-mail: takalloozadeh@shirazu.ac.ir

Gil ho Yoon[1]
Engineering Center 202-2,
Hanyang University,
222 Wangsimni-ro,
Seoul, Seong dong-gu 133-791, Korea
e-mails: ghy@hanyang.ac.kr,
gilho.yoon@gmail.com

The creep phenomenon has enormous effect on the stress and displacement distribution in the structures. Redistribution of the stress field is one of these effects which is called stress relaxation. The importance of stress relaxation in the design of structures is increasing due to engineering applications especially in high temperature. However, this phenomenon has remained absent from the structural optimization studies. In the present study, the effect of stress relaxation due to high temperature creep is considered in topology optimization (TO). Internal element connectivity parameterization (I-ECP) method is utilized for performing TO. This method is shown to be effective to overcome numerical instabilities in nonlinear problems. Time-dependent adjoint sensitivity formulation is implemented for I-ECP including creep effect. Several benchmark problems are solved, and the optimum layouts obtained by linear and nonlinear methods are compared to show the efficiency of the proposed method and to show the effect of stress relaxation on the optimum layout. [DOI: 10.1115/1.4041578]

Keywords: topology optimization, stress relaxation, element connectivity parameterization, nonlinear finite element analysis, creep

1 Introduction

The main purpose of this study is considering the effect of the stress relaxation at high temperature creep on the optimum layout of the structures. The steady-state creep is modeled as an ascending function of stress. Therefore, parts of the structure with more stress are under more creep effect. Stress relaxation causes changes in the stress distribution, reduction of the maximum stress, and increment in the displacement. These changes happen over time and they are the function of temperature as well. Figure 1 shows the creep deformation in an old wood structure. This unwanted deformation can disrupt the performance of the structures. Experimental tests indicate that the creep effect has three main periods and continues until the rupture of the structure. This issue is discussed in Secs. 1.3 and 2.1.

1.1 Topology Optimization and Material Nonlinearity Problems. Today, topology optimization (TO) is widely used as a powerful tool in structural optimization. It has been well developed to obtain the optimum layout for structural and nonstructural problems. Based on the governing equation, these problems can be divided into linear and nonlinear problems. In the structural problems, nonlinearity can be due to nonlinear behavior of materials or large deformation which is called geometrical nonlinearity. Moreover, there is contact nonlinearity which is due to the contact of different parts of the structure. Material nonlinearity is including any inelastic behavior of material and is categorized as rate-independent and rate-dependent nonlinearity [1]. Nonlinear elasticity behavior, buckling, and plasticity behavior are in the first category and viscoelasticity, visco-plasticity, fatigue, and creep are classified in the rate-dependent nonlinearity (Fig. 2).

Although TO was introduced to solve linear structural problems, it was rapidly developed to consider nonlinearity aspects of structures. However, most studies have focused on large deformation behavior especially in mechanism problems since the displacements of mechanisms are intrinsically large [2]. The first studies which investigated nonlinearity in TO were performed by homogenization [3,4] approach. Swan and Kosaka demonstrated that the optimal layout for maximal strength considering nonlinearity can be significantly different from the layout for minimal elastic compliance [5]. As a popular method in TO, solid isotropic material with penalization method (SIMP) [6] is utilized in solving structural nonlinearity by Jung and Gea [7]. Green–Lagrange strain tensor and second Piolar–Kirchhoff stress tensor were used to express strain and stress in large deformation, respectively, and generalized convex approximation is utilized in TO.

Fig. 1 Deformations due to creep effect in a wood structure (Braunschweig, Germany)

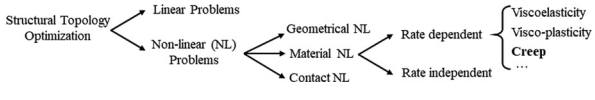

Fig. 2 Creep in structural TO problems category

[1]Corresponding author.

Contributed by the Design Engineering Division of ASME for publication in the Journal of Computational and Nonlinear Dynamics. Manuscript received April 17, 2018; final manuscript received September 20, 2018; published online January 7, 2019. Assoc. Editor: Kyung Choi.

In both geometric and material nonlinearities, several instabilities and difficulties are reported. These problems are mostly in the analysis step but not in the sensitivity or optimization part. In addition to the computational cost, one difficulty in considering nonlinearity in SIMP method is the problem of indefinite or even negative definite tangent stiffness matrix in low-density elements [8,9]. This is due to large displacements during TO process. To overcome this problem, one might remove low-density elements [10]. Another method is relaxation of the convergence criteria [8]. Huang and Xie [11] proposed modified bidirectional evolutionary structural optimization method to solve this problem in topology optimization of nonlinear structures which is based on removing and adding elements. In their study, a new scheme for ranking solid and void elements is used. Significant improvements in results are obtained. However, the oscillation between designs of two different deformation states is reported due to nonlinearity and partial unloading of material. Another approach is equivalent static loads method which is proposed in Ref. [9] to consider different kinds of nonlinear static response in TO. In this method, after nonlinear analysis, equivalent static loads are calculated and linear static topology optimization was performed [12]. Using multi-scale TO is an other novel approach in nonlinear structural design [13–15]. More recently, the effect of void elements such as layering and islanding is investigated [16]. The proposed algorithm is based on performing all finite element (FE) analyses for subdomains with solid and gray elements via removing all void elements. In a different approach, a discrete filtering scheme is utilized to remove spurious members in topology optimization of truss lattices [17].

Another popular method in TO is based on level-set [18–20]. Considering geometric nonlinearity in level-set based TO is reported by using unstructured mesh [21] in which the convergence difficulty is significantly relieved.

One of the obstacles related to low density is excessive mesh distortion which causes problems in convergence of the optimization. A method which is proved to be efficient to overcome this problem and the other instability problem in nonlinear TO is element connectivity (ECP) method [22,23]. This method is described in the next section and utilized in this study.

1.2 Internal Element Connectivity Parameterization Approach. The internal element connectivity parameterization (I-ECP) method [22,24–30] is an efficient method to circumvent numerical instabilities in nonlinear problems related to low-stiffness elements. In this method, the elements are solid (in contrast to SIMP) but they are connected by zero-length links. Design variables define the stiffness of these links. There are two modeling techniques in ECP method: external ECP [22,24] and I-ECP [26,27]. The difference is in links location, while in external ECP, elements do not share nodes and they are connected by external links, in I-ECP, internal links are used to connect element to the shared nodes. Figure 2 depicts an element in I-ECP method. Here, the stiffness matrix of solid element e is $\mathbf{k}_{\text{str}}^{e}$ which is connected by one-dimensional zero-length links with stiffness l^e to the finite element nodes. The degrees-of-freedom of the internal nodes defining the finite element are eliminated by the static condensation technique. Therefore, the number of assembled nodes in the global stiffness matrix is exactly the same as that required for the SIMP method. The details of FE computations are given in Sec. 2.2.

1.3 Stress Relaxation in Creep. The behavior of the most materials can be well described by the theory of elasticity. However, at high temperature conditions, the importance of creep is revealed. The increasing use of high temperature equipment represents the importance and urgent need of design under creep effect. It was first noticed in the development and design of turbines [31]. Today, the theory of creep for different materials and condition is well developed and there are lots of formulation to define this effect under different situations. The behavior under creep can be divided into three stages as the primary, secondary, and tertiary creep stages [32]. A typical creep curve is shown in Fig. 4. This division is based on the decreasing, constant, and increasing creep strain rates, respectively.

Despite the significant progress in the theory of creep, there are few studies in considering creep or viscoelasticity in TO. Among rate-dependent material nonlinearity, viscoelastic TO has been studied sporadically mostly as viscoelastic damping [33]. However, there are several studies that investigated nonlinear continuum damage models in TO [34,35]. Recently, James and Waisman [36] performed TO for viscoelastic creep deformation. A linear viscoelastic model is utilized in standard TO (SIMP) and time-dependent adjoint method is used for sensitivity analysis. The results show high dependency of optimal layout to the load duration. In their study, Prony series function is utilized to define Young's modules as a function of time.

Despite the mentioned studies, there is a significant void within the nonlinear TO in considering creep effects such as stress relaxation. Creep is a complex function of time, stress, and temperature. Considering whole, these complexities in TO would be an open field of research. In this paper, we investigate the effect of creep stress relaxation on optimal design. The proposed method obtained the optimal layout at the end of the secondary stage under constant load. To this end, a creep stress relaxation theory is utilized which leads to increment in the displacement field and alleviates the maximum stress in the structure. Section 2 describes the formulation of the used stress relaxation theory and finite element implementation. In Sec. 3, sensitivity analysis for using in I-ECP is derived. The results and discussion are given in Sec. 4, and finally, conclusion is presented in Sec. 5.

2 Mathematical Formulation for Creep and Internal Element Connectivity Parameterization

In this section, the theory of stress relaxation creep which is used in this study is presented. Moreover, a brief review of I-ECP method is given, and then, implementation of the stress relaxation in finite element analysis by I-ECP method is described.

2.1 Stress Relaxation Formulation. Creep is a time-dependent stress–strain relation, and in general, it is the function of time (t), stress (σ), and temperature (T) [31] which can be written as following mathematical form:

$$\varepsilon_{\text{creep}} = f(t,\sigma,T) = f_1(t)f_2(\sigma)f_3(T) \tag{1}$$

In the above relation, it was assumed that each function depends on only one variable. The aim of this study is to optimally design the structures during secondary stage when the stress distribution is changed due to the creep effect. The primary stage is almost fast and the tertiary stage leads to rupture but the secondary stage is a steady-state which covers the most period of the life of the structure. By assuming the constant temperature, the creep strain that causes stress relaxation can be written just as a function of the stress

$$\varepsilon_{\text{creep}} = f(\sigma) \tag{2}$$

Many researchers have investigated the above relation mainly for the secondary stage of the creep. For both metal and alloys, the secondary creep rate ($\dot{\varepsilon}$) can be expressed by a power relation [31,37]

$$\dot{\varepsilon} = \alpha\sigma^{z} \tag{3}$$

Here, the parameters α and z are material properties' parameters. There are some other relations such as $\alpha(e^{(\sigma/\sigma_0)}-1)$ and $\alpha(\sinh(\sigma/\sigma_0))^z$[38]; however, it does not have effect on generality of our optimization method and one can use different relations for

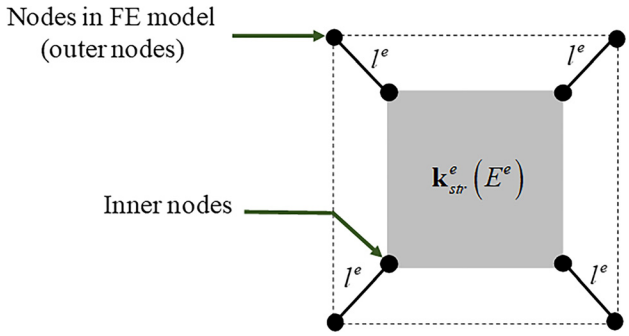

Fig. 3 An element in I-ECP

creep strain in the present TO method just by changing Eq. (4) in FE analysis and Eq. (41) in sensitivity analysis.

The appropriate range for z in annealed metals is between 1 and 7 [31,39]. In most cases of creep at high temperature and for alloys, z varies between 2 and 4 [31]. The total strain at the arbitrary time ($t = t_f$) can be obtained as summation of elastic and creep strains

$$\varepsilon = \frac{\sigma}{E_0} + \alpha\sigma^z t_f = \sigma\left(\frac{1}{E_0} + \alpha\sigma^{z-1}t_f\right) \Rightarrow \frac{\sigma}{\varepsilon} = \frac{E_0}{1+\alpha t_f E_0 \sigma^{z-1}} \Rightarrow E = \frac{E_0}{1+\beta\sigma^m} \tag{4}$$

The above relation is called strain hardening and we used the assumption of constant slope of the creep strain curve in the secondary stage. The intensity of stress relaxation and the desired time for design (t_f) are seen in the parameter β which is equal to $\alpha t_f E_0$. Moreover, $z-1$ is replaced by m for the convenience of calculations. As shown in Eq. (4), the points with higher stress have lower stiffness and this tends to redistribution of stress and displacement field in the structure which is called stress relaxation. Equation (4) is obtained from uniaxial test but it can generalize for stress relaxation in multi-axial stress state [40]. The equivalent effect of a multi-axial stress system has been achieved through the concept of yield criterion [38]. Von Mises yield criterion (σ_v) is commonly assumed as the effective stress.

2.2 Internal Element Connectivity Parameterization Formulation. The details of computations of I-ECP method can be found in Ref. [26]. Here, we provide a summary of calculation which is used in this research. Assume an element in I-ECP method that is depicted in Fig. 3. The shown (zero-length) four links have different values for stiffness. However, to reduce the number of design variables, we used one stiffness value (l^e) for each element. Therefore, by using $\mathbf{k}^e_l = l^e\mathbf{I}_{8\times8}$ for planar element, the stiffness matrix and equilibrium equation for element e can be written as

$$\begin{bmatrix} \mathbf{k}^e_l & -\mathbf{k}^e_l \\ -\mathbf{k}^e_l & \mathbf{k}^e_l + \mathbf{k}^e_{\text{str}} \end{bmatrix} \begin{Bmatrix} \mathbf{u}^e_{\text{out}} \\ \mathbf{u}^e_{\text{in}} \end{Bmatrix} = \begin{Bmatrix} \mathbf{f}^e_{\text{out}} \\ \mathbf{f}^e_{\text{in}} \end{Bmatrix} \tag{5}$$

The indices in and out represent the inner and outer node's force or displacement, respectively. Note that all elements in the inner force vector ($\mathbf{f}^e_{\text{in}}$) are zero. Here, $\mathbf{k}^e_{\text{str}}$ is the stiffness of the solid element inside the I-ECP element. This stiffness is only the function of Young's modulus and not design variables. To reduce the total degree-of-freedom of the system and computational cost, static condensation scheme was proposed [26]. The results are given here for the relation between inner and outer displacements

$$\mathbf{u}^e_{\text{in}} = (\mathbf{k}^e_l + \mathbf{k}^e_{\text{str}})^{-1}\mathbf{k}^e_l\mathbf{u}^e_{\text{out}} \tag{6}$$

After some calculation using Woodbury formula, the condensed stiffness matrix ($\mathbf{k}^e_{\text{con}}$) would be obtained as follows:

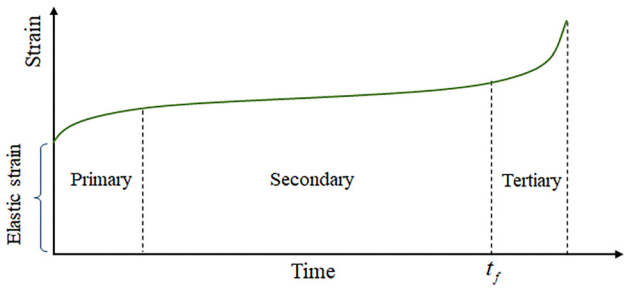

Fig. 4 Typical creep curve

$$\mathbf{k}^e_{\text{con}} = \mathbf{k}^e_{\text{str}}\left(\mathbf{I}_{8\times8} + \frac{1}{l^e}\mathbf{k}^e_{\text{str}}\right)^{-1} \tag{7}$$

When condensed stiffness matrix is calculated, the relation between outer displacement and force vectors can be written as

$$\mathbf{k}^e_{\text{con}}\mathbf{u}^e_{\text{out}} = \mathbf{f}^e_{\text{out}} \tag{8}$$

The final step is assembling the stiffness matrix and load vector and then solving the following linear equation system, to achieve the displacement field:

$$\mathbf{K}_{\text{con}}\mathbf{U}_{\text{out}} = \mathbf{F}_{\text{out}} \tag{9}$$

Moreover, the following interpolation function is used to map design variable of the eth element (x^e) which varies between zero and one into the stiffness of zero-length links (l^e):

$$l^e = \frac{(l_{\max} - l_{\min})(x^e)^p}{1 + (1-(x^e)^p)\dfrac{(l_{\max} - l_{\min})}{k^{\text{diag}}_{\text{str}} \times 2}} + l_{\min} \tag{10}$$

The values for upper bound ($l_{\max}$) and lower bound ($l_{\min}$) are chosen as 10^4 and 10^{-4}, respectively. In addition, p is the penalty function, which is equal to 3. $k^{\text{diag}}_{\text{str}}$ is the average of diagonal elements in stiffness matrix of solid element. This value is constant in this study since we use a uniform mesh ($sdiag = k^{\text{diag}}_{\text{str}} \times 2 = \text{const.}$).

2.3 Nonlinear Finite Element Implementation. To obtain the displacement and stress field, a step-by-step algorithm is performed for nonlinear finite element analysis. Figure 5 depicts the schematic of analysis procedure. The applied force ($\mathbf{F}_s$) is increased gradually and Young's modulus of each element is updated after calculating von Mises stress field at each step. Index s stands for the number of step and the total number of steps is n. It should be mentioned that β is the function of material property (α) and the lifetime of the structure (t_f) but not time-step in nonlinear analysis. Therefore, it is constant during nonlinear analysis. The stiffness matrix of solid element inside each I-ECP element is obtained as follows:

$$\mathbf{k}^e_{\text{str}} = E^e\int \mathbf{B}^{\text{T}}\mathbf{D}\mathbf{B}d\Omega^e, \quad E^e = \frac{E_0}{1+\beta\sigma^m_v} \tag{11}$$

Here, $\mathbf{D}$ represents material tensor, $\mathbf{B}$ stands for gradient matrix, and von Mises can be written in the form of stress components (σ_{ij}) for 2D problems

$$\sigma_v = \sqrt{\sigma^2_{11} + \sigma^2_{22} - \sigma_{11}\sigma_{22} + 3\sigma^2_{12}} \tag{12}$$

A cantilever beam (Fig. 6) is analyzed under a unit concentrated load by the aforementioned algorithm with 10 steps ($n = 10$).

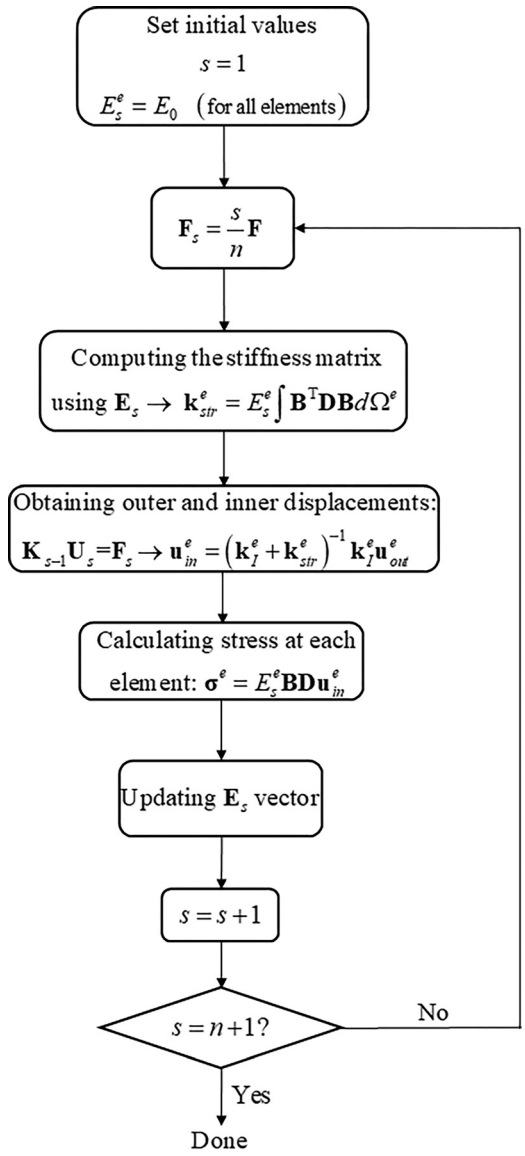

Fig. 5 Schematic diagram for nonlinear analyzing algorithm

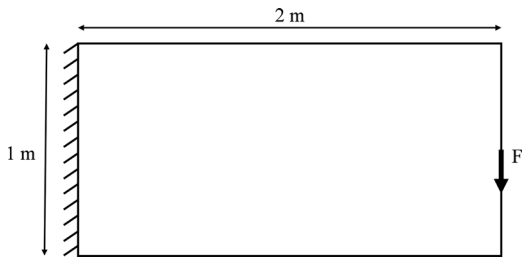

Fig. 6 Cantilever beam problem

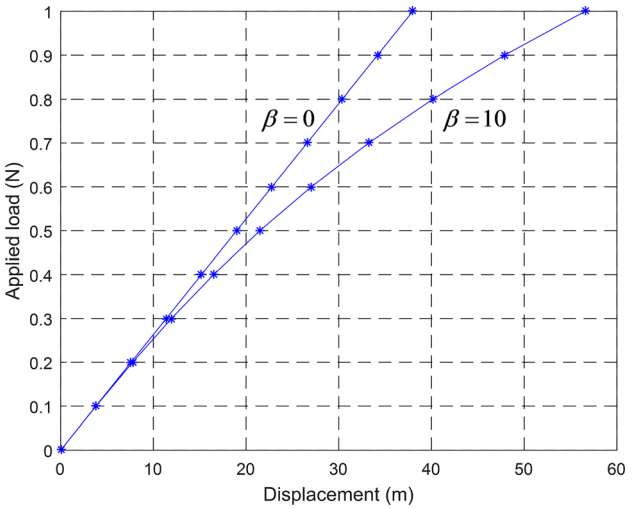

Fig. 8 Displacement—Load history at load point ($\beta = 0$ and $\beta = 10$)

Initial Young's modulus is $E_0 = 1\,\mathrm{N/m^2}$ and $\nu = 0.3$ is selected for the Poisson ratio. The following relation by selecting $\beta = 10$ and $m = 2$ is used to update the Young modulus values:

$$E^e = \frac{1}{1 + 10\sigma_v^2} \tag{13}$$

The obtained stress field in the domain for this problem and for the linear analysis problem ($\beta = 0$) is shown in Fig. 7. In addition, the displacement values at the tip of the cantilever beam for both linear and nonlinear analyses are plotted in Fig. 8. As it can be seen, the maximum stress is reduced about 18.8% due to the stress relaxation and the stress field has become smoother. Moreover, the maximum displacement is increased which leads to the increment in stored strain energy in the structure.

3 Optimization Formulation and Sensitivity Analysis

Stored strain energy is selected as the objective function. This is the area under displacement-force curve in Fig. 8

$$\begin{aligned} C = \int_\Omega \mathbf{u}\cdot d\mathbf{f} &= \sum_{s=1}^{n}(\mathbf{U}_s - \mathbf{U}_{s-1})^T\left(\frac{\mathbf{F}_s + \mathbf{F}_{s-1}}{2}\right) \\ &= \sum_{s=1}^{n}(\mathbf{U}_s - \mathbf{U}_{s-1})^T\left(\frac{2s-1}{2n}\right)\mathbf{F} \\ &= \sum_{s=1}^{n}(\mathbf{U}_s - \mathbf{U}_{s-1})^T\left(\frac{s}{n}\right)\mathbf{F} - \frac{1}{2n}\sum_{s=1}^{n}(\mathbf{U}_s - \mathbf{U}_{s-1})^T\mathbf{F} \\ &= (\mathbf{U}_n)^T\mathbf{F} - \frac{1}{n}\sum_{s=1}^{n-1}(\mathbf{U}_s)^T\mathbf{F} - \frac{1}{2n}(\mathbf{U}_n)^T\mathbf{F} \\ &= \frac{2n-1}{2n}(\mathbf{U}_n)^T\mathbf{F} - \frac{1}{n}\sum_{s=1}^{n-1}(\mathbf{U}_s)^T\mathbf{F} \end{aligned} \tag{14}$$

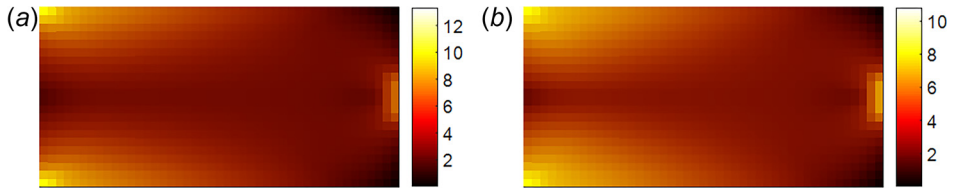

Fig. 7 von Mises stress field for (*a*) $\beta = 0$ ($\sigma_{max} = 13.2827\,\mathrm{N/m^2}$) and (*b*) $\beta = 10$($\sigma_{max} = 10.7875\,\mathrm{N/m^2}$)

Here, s shows the number of step and n is the total number of steps in nonlinear finite element analysis. Using the above objective function, the TO problem can be formulated as follows:

$$\begin{aligned} &\underset{\Omega\subset D}{\text{Min}} \quad \{\text{Strain energy}\} = C \\ &\text{Subject to}: \\ &\quad |\Omega| = |\Omega|^* \\ &\quad \mathbf{K}_{\text{con}}\mathbf{U}_{\text{out}} = \mathbf{F}_{\text{out}} \end{aligned} \tag{15}$$

Here, Ω is a topology that must be computed within the design domain and $|\Omega|^*$ is the final volume fraction.

3.1 Sensitivity Analysis Using Time-Dependent Adjoint Method. Sensitivity analysis by utilizing adjoint method is performed in this section. To this end, we add the objective function with the summation of equilibrium equation at all steps of analysis multiplied to an arbitrary adjoint vector ($\boldsymbol{\lambda}_s$). Therefore, the sensitivity of the stored strain energy with respect to arbitrary design variable x is

$$\begin{aligned} C &= \frac{2n-1}{2n}(\mathbf{U}_n)^{\mathrm{T}}\mathbf{F} - \frac{1}{n}\sum_{s=1}^{n-1}(\mathbf{U}_s)^{\mathrm{T}}\mathbf{F} + \sum_{s=1}^{n}\boldsymbol{\lambda}_s(\mathbf{K}_{s-1}\mathbf{U}_s - \mathbf{F}_s) \\ \Rightarrow \frac{dC}{dx} &= \frac{2n-1}{2n}\left(\frac{d\mathbf{U}_n}{dx}\right)^{\mathrm{T}}\mathbf{F} - \frac{1}{n}\sum_{s=1}^{n-1}\left(\frac{d\mathbf{U}_s}{dx}\right)^{\mathrm{T}}\mathbf{F} \\ &\quad + \sum_{s=1}^{n}\boldsymbol{\lambda}_s\left(\frac{d\mathbf{K}_{s-1}}{dx}\mathbf{U}_s + \mathbf{K}_{s-1}\frac{d\mathbf{U}_s}{dx}\right) \end{aligned} \tag{16}$$

For the sake of simplicity, we removed the index con for the condensed stiffness matrix. Considering stress relaxation, the stiffness matrix is the function of both design variables (x) and Young's modulus. Applying the chain rule, we have

$$\begin{aligned} &\boldsymbol{\lambda}_s\frac{d\mathbf{K}_{s-1}(x,\mathbf{U}_{s-1})}{dx}\mathbf{U}_s \\ &= \sum_{e=1}^{\text{nele}}\boldsymbol{\lambda}_s^e\frac{d\mathbf{k}_{s-1}^e}{dx}\mathbf{u}_s^e = \sum_{e=1}^{\text{nele}}\boldsymbol{\lambda}_s^e\left[\frac{\partial\mathbf{k}_{s-1}^e}{\partial x} + \frac{\partial\mathbf{k}_{s-1}^e}{\partial E_{s-1}^e}\times\frac{dE_{s-1}^e}{dx}\right]\mathbf{u}_s^e \\ &= \sum_{e=1}^{\text{nele}}\boldsymbol{\lambda}_s^e\frac{\partial\mathbf{k}_{s-1}^e}{\partial x}\mathbf{u}_s^e + \boldsymbol{\lambda}_s^e\frac{\partial\mathbf{k}_{s-1}^e}{\partial E_{s-1}^e}\mathbf{u}_s^e\times\frac{dE_{s-1}^e}{dx} \\ &= \sum_{e=1}^{\text{nele}}\boldsymbol{\lambda}_s^e\frac{\partial\mathbf{k}_{s-1}^e}{\partial x}\mathbf{u}_s^e + q_s^e\times\frac{dE_{s-1}^e}{dx} \end{aligned} \tag{17}$$

Here, $n$ele is the number of elements in FE model and q_s^e in each step is defined as follows:

$$q_s^e = \boldsymbol{\lambda}_s^e\frac{\partial\mathbf{k}_{s-1}^e}{\partial E_{s-1}^e}\mathbf{u}_s^e \tag{18}$$

On the other hand

$$\begin{aligned} \frac{dE_{s-1}^e}{dx} &= \frac{dE_{s-1}^e}{d\sigma_{s-1}^e}\times\frac{d\sigma_{s-1}^e}{dx} \\ &= \frac{dE_{s-1}^e}{d\sigma_{s-1}^e}\times\left(\sum_{i=1}^{8}\left(\frac{\partial\sigma_{s-1}^e}{\partial\mathbf{u}_{s-1}^{\text{in}}(i)}\times\frac{d\mathbf{u}_{s-1}^{\text{in}}(i)}{dx}\right) + \frac{\partial\sigma_{s-1}^e}{\partial E_{s-2}^e}\times\frac{dE_{s-2}^e}{dx}\right) \end{aligned} \tag{19}$$

We can write the above equation in the vector form

$$\frac{dE_{s-1}^e}{dx} = \frac{dE_{s-1}^e}{d\sigma_{s-1}^e}\times\left(\left(\frac{\partial\sigma_{s-1}^e}{\partial\mathbf{u}_{s-1}^{\text{in}}}\right)^{\mathrm{T}}\times\frac{d\mathbf{u}_{s-1}^{\text{in}}}{dx} + \frac{\partial\sigma_{s-1}^e}{\partial E_{s-2}^e}\times\frac{dE_{s-2}^e}{dx}\right) \tag{20}$$

The derivative of inner displacement with respect to design variable is obtained as follows:

$$\begin{aligned} \mathbf{u}_{s-1}^{\text{in}} &= (\mathbf{k}_I^e + \mathbf{k}_{\text{str}}^e)^{-1}\mathbf{k}_I^e\mathbf{u}_{s-1}^{\text{out}} \Rightarrow (\mathbf{k}_I^e + \mathbf{k}_{\text{str}}^e)\mathbf{u}_{s-1}^{\text{in}} \\ &= \mathbf{k}_I^e\mathbf{u}_{s-1}^{\text{out}} \Rightarrow \frac{dl^e}{dx}\mathbf{u}_{s-1}^{\text{in}} + \frac{dE_{s-2}^e}{dx}\mathbf{k}_{\text{str}}^e\mathbf{u}_{s-1}^{\text{in}} + (\mathbf{k}_I^e + \mathbf{k}_s^e)\frac{d\mathbf{u}_{s-1}^{\text{in}}}{dx} \\ &= \frac{dl^e}{dx}\mathbf{u}_{s-1}^{\text{out}} + l^e\frac{d\mathbf{u}_{s-1}^{\text{out}}}{dx} \Rightarrow \frac{d\mathbf{u}_{s-1}^{\text{in}}}{dx} \\ &= (\mathbf{k}_I^e + \mathbf{k}_{s-2}^e)^{-1} \\ &\quad\times\left(\frac{dl^e}{dx}(\mathbf{u}_{s-1}^{\text{out}} - \mathbf{u}_{s-1}^{\text{in}}) - \frac{dE_{s-2}^e}{dx}\mathbf{k}_{\text{str}}^e\mathbf{u}_{s-1}^{\text{in}} + l^e\frac{d\mathbf{u}_{s-1}^{\text{out}}}{dx}\right) \end{aligned} \tag{21}$$

Substituting in Eq. (20), we have

$$\begin{aligned} &\frac{dE_{s-1}^e}{dx} \\ &= \frac{dE_{s-1}^e}{d\sigma_{s-1}^e}\times\left(\left(\frac{\partial\sigma_{s-1}^e}{\partial\mathbf{u}_{s-1}^{\text{in}}}\right)^{\mathrm{T}}\times(\mathbf{k}_I^e + \mathbf{k}_{s-2}^e)^{-1}\left(\frac{dl^e}{dx}(\mathbf{u}_{s-1}^{\text{out}} - \mathbf{u}_{s-1}^{\text{in}})\right.\right. \\ &\left.\left. - \frac{dE_{s-2}^e}{dx}\mathbf{k}_{\text{solid}}\mathbf{u}_{s-1}^{\text{in}} + l^e\frac{d\mathbf{u}_{s-1}^{\text{out}}}{dx}\right) + \frac{\partial\sigma_{s-1}^e}{\partial E_{s-2}^e}\times\frac{dE_{s-2}^e}{dx}\right) \end{aligned} \tag{22}$$

The above relation is written in simple form as follows:

$$\frac{dE_{s-1}^e}{dx} = A_{s-1}^e\frac{dE_{s-2}^e}{dx} + B_{s-1}^e + \mathbf{V}_{s-1}^e\frac{d\mathbf{u}_{s-1}^{\text{out}}}{dx} \tag{23}$$

where

$$\begin{aligned} A_{s-1}^e &= \frac{dE_{s-1}^e}{d\sigma_{s-1}^e}\times\frac{\partial\sigma_{s-1}^e}{\partial E_{s-2}^e} - \frac{dE_{s-1}^e}{d\sigma_{s-1}^e}\left(\frac{d\sigma_{s-1}^e}{d\mathbf{u}_{s-1}^{\text{in}}}\right)^{\mathrm{T}} \\ &\quad\times\left((\mathbf{k}_I^e + \mathbf{k}_{s-2}^e)^{-1}\times(\mathbf{k}_{\text{solid}}\mathbf{u}_{s-1}^{\text{in}})\right) \end{aligned} \tag{24}$$

$$\begin{aligned} B_{s-1}^e &= \frac{dE_{s-1}^e}{d\sigma_{s-1}^e}\left(\frac{d\sigma_{s-1}^e}{d\mathbf{u}_{s-1}^{\text{in}}}\right)^{\mathrm{T}} \\ &\quad\times\left((\mathbf{k}_I^e + \mathbf{k}_{s-2}^e)^{-1}\times\frac{dl^e}{dx}(\mathbf{u}_{s-1}^{\text{out}} - \mathbf{u}_{s-1}^{\text{in}})\right) \end{aligned} \tag{25}$$

$$\mathbf{V}_{s-1}^e = \frac{dE_{s-1}^e}{d\sigma_{s-1}^e}\times\left(\left(\frac{d\sigma_{s-1}^e}{d\mathbf{u}_{s-1}^{\text{in}}}\right)^{\mathrm{T}}(\mathbf{k}_I^e + \mathbf{k}_{s-2}^e)^{-1}l^e\right) \tag{26}$$

Substituting Eq. (23) in Eq. (17) yields

$$\begin{aligned} \boldsymbol{\lambda}_s\frac{d\mathbf{K}_{s-1}(x,\mathbf{U}_{s-1})}{dx}\mathbf{U}_s &= \sum_{e=1}^{\text{nele}}\boldsymbol{\lambda}_s^e\frac{\partial\mathbf{k}_{s-1}^e}{\partial x}\mathbf{u}_s^e + q_s^e \\ &\quad\times\left(A_{s-1}^e\frac{dE_{s-2}^e}{dx} + B_{s-1}^e + \mathbf{V}_{s-1}^e\frac{d\mathbf{u}_{s-1}^{\text{out}}}{dx}\right) \end{aligned} \tag{27}$$

Therefore, there is a recurrence relation to define the coefficient for (dE_{s-2}^e/dx)

$$q_{s-1}^e = \boldsymbol{\lambda}_{s-1}^e\frac{\partial\mathbf{k}_{s-2}^e}{\partial E_{s-2}^e}\mathbf{u}_{s-1}^e + q_s^eA_{s-1}^e \tag{28}$$

Finally, Eq. (17) would be obtained

$$\boldsymbol{\lambda}_s \frac{d\mathbf{K}_{s-1}(x,\mathbf{U}_{s-1})}{dx}\mathbf{U}_s = \sum_{e=1}^{\text{nele}} \boldsymbol{\lambda}_s^e \frac{\partial \mathbf{k}_{s-1}^e}{\partial x}\mathbf{u}_s^e + \left(q_s^e A_{s-1}^e \frac{dE_{s-2}^e}{dx} + h_{s-1}^e + \mathbf{p}_{s-1}^e \frac{d\mathbf{u}_{s-1}^{\text{out}}}{dx}\right) \tag{29}$$

Here, $\mathbf{p}_{s-1}^e$ and h_{s-1}^e are defined as follows:

$$\begin{aligned} \mathbf{p}_{s-1}^e &= q_s^e \times \mathbf{V}_{s-1}^e \\ h_{s-1}^e &= q_s^e \times B_{s-1}^e \end{aligned} \tag{30}$$

Substituting in Eq. (16), the desired derivative will be written as follows:

$$\frac{dC}{dx} = \frac{2n-1}{2n}\left(\frac{d\mathbf{U}_n}{dx}\right)^{\mathrm{T}}\mathbf{F} - \frac{1}{n}\sum_{s=1}^{n-1}\left(\frac{d\mathbf{U}_s}{dx}\right)^{\mathrm{T}}\mathbf{F} + \sum_{s=1}^{n}\left(\boldsymbol{\lambda}_s \frac{\partial \mathbf{K}_{s-1}}{\partial x}\mathbf{U}_s + H_{s-1} + \mathbf{P}_{s-1}\frac{d\mathbf{U}_{s-1}}{dx} + \boldsymbol{\lambda}_s \mathbf{K}_{s-1}\frac{d\mathbf{U}_s}{dx}\right) \tag{31}$$

To vanish the terms with coefficient $(d\mathbf{U}_n/dx)$, the following relation must be established:

$$\frac{2n-1}{2n}\left(\frac{d\mathbf{U}_n}{dx}\right)^{\mathrm{T}}\mathbf{F} + \boldsymbol{\lambda}_n^{\mathrm{T}}\left(\mathbf{K}_{n-1}\frac{d\mathbf{U}_n}{dx}\right) = 0 \Rightarrow \mathbf{K}_{n-1}\boldsymbol{\lambda}_n = -\frac{2n-1}{2n}\mathbf{F} \tag{32}$$

and for vanishing the terms with coefficient $(d\mathbf{U}_s/dx)$, we need

$$-\frac{1}{n}\sum_{s=1}^{n-1}\left(\frac{d\mathbf{U}_s}{dx}\right)^{\mathrm{T}}\mathbf{F} + \sum_{s=1}^{n}\left(\mathbf{P}_{s-1}^{\mathrm{T}}\frac{d\mathbf{U}_{s-1}}{dx} + \boldsymbol{\lambda}_n^{\mathrm{T}}\mathbf{K}_{s-1}\frac{d\mathbf{U}_s}{dx}\right) = 0 \Rightarrow \mathbf{K}_{s-1}\boldsymbol{\lambda}_s = \frac{1}{n}\mathbf{F} - \mathbf{P}_{s-1} \quad (s = 1,2,\ldots,n-1) \tag{33}$$

After solving Eqs. (32) and (33), adjoint vector $(\boldsymbol{\lambda}_s)$ will be obtained. Then, the desired sensitivity will be calculated as follows:

$$\frac{dC}{dx} = \sum_{s=1}^{n}\boldsymbol{\lambda}_s^{\mathrm{T}}\left(\frac{\partial \mathbf{K}_{s-1}}{\partial x} + \mathbf{H}_{s-1}\right)\mathbf{U}_s \tag{34}$$

In the above relations, the stiffness matrix of each element is defined as Eq. (7). Therefore

$$\frac{\partial \mathbf{K}}{\partial x} = \frac{\partial \mathbf{k}^e}{\partial x} = \frac{\partial \mathbf{k}^e}{\partial l^e}\times\frac{dl^e}{dx} \tag{35}$$

The first term in the derivative can be obtained from recasting the stiffness matrix

$$\begin{aligned} &\mathbf{k}^e = \mathbf{k}_{\text{str}}^e\left(\mathbf{I} + \frac{1}{l^e}\mathbf{k}_{\text{str}}^e\right)^{-1} \Rightarrow \left(\mathbf{I} + \frac{1}{l^e}\mathbf{k}_{\text{str}}^e\right)\mathbf{k}^e = \mathbf{k}_{\text{str}}^e \\ &\Rightarrow l^e\mathbf{k}^e + \mathbf{k}_s^e\mathbf{k}^e = l^e\mathbf{k}_{\text{str}}^e \Rightarrow \mathbf{k}^e + l^e\left(\frac{\partial \mathbf{k}^e}{\partial l^e}\right) + \mathbf{k}_s^e\left(\frac{\partial \mathbf{k}^e}{\partial l^e}\right) = \mathbf{k}_{\text{str}}^e \\ &\Rightarrow (l^e\mathbf{I} + \mathbf{k}_{\text{str}}^e)\left(\frac{\partial \mathbf{k}^e}{\partial l^e}\right) = \mathbf{k}_{\text{str}}^e - \mathbf{k}^e \Rightarrow \frac{\partial \mathbf{k}^e}{\partial l^e} = (\mathbf{k}_{\text{str}}^e - \mathbf{k}^e)(l^e\mathbf{I} + \mathbf{k}_{\text{str}}^e)^{-1} \end{aligned} \tag{36}$$

The second term of derivative in Eq. (35) will be obtained easily as follows:

$$\frac{dl^e}{dx} = \frac{n(l_{\max} - l_{\min})x^{n-1}}{1 + (1-x^n)\dfrac{(l_{\max} - l_{\min})}{k_s^{\text{diag}} \times 2}} - \frac{(l_{\max} - l_{\min})x^n \times \left(-\dfrac{n(l_{\max} - l_{\min})}{k_s^{\text{diag}} \times 2}x^{n-1}\right)}{\left(1 + (1-x^n)\dfrac{(l_{\max} - l_{\min})}{k_s^{\text{diag}} \times 2}\right)^2} \tag{37}$$

In Eq. (19), the sensitivity of the von Mises stress in each element with respect to inner displacement at degree-of-freedom i needs to be calculated. From the definition of von Mises stress in 2D plane stress (Eq. (12)), we have

$$\frac{\partial \sigma^e}{\partial \mathbf{u}^{\text{in}}(i)} = \left(\frac{E^e}{2\sigma^e}\right) \times \left((\mathbf{DB})_{1,i}(2\sigma_{11} - \sigma_{22}) + (\mathbf{DB})_{2,i}(2\sigma_{22} - \sigma_{11}) + 6(\mathbf{DB})_{3,i}\sigma_{12}\right) \tag{38}$$

Here, $(\mathbf{DB})_{j,i}$ represents the jth row and the ith column of $\mathbf{DB}$ matrix. Moreover, in Eq. (18), the derivative of the condensed element stiffness with respect to Young's modulus $(\partial \mathbf{k}^e/\partial E^e)$ will be obtained by using Eq. (7)

$$\begin{aligned} &\mathbf{k}^e = \mathbf{k}_{\text{str}}^e\left(\mathbf{I} + \frac{1}{l^e}\mathbf{k}_{\text{str}}^e\right)^{-1} \Rightarrow \left(\mathbf{I} + \frac{1}{l^e}\mathbf{k}_{\text{str}}^e\right)\mathbf{k}^e = \mathbf{k}_{\text{str}}^e \\ &\Rightarrow l^e\mathbf{k}^e + \mathbf{k}_{\text{str}}^e\mathbf{k}^e = l^e\mathbf{k}_{\text{str}}^e \\ &\Rightarrow l^e\frac{\partial \mathbf{k}^e}{\partial E^e} + \frac{\partial \mathbf{k}_{\text{str}}^e}{\partial E^e}\mathbf{k}^e + \mathbf{k}_{\text{str}}^e\frac{\partial \mathbf{k}^e}{\partial E^e} = l^e\frac{\partial \mathbf{k}_{\text{str}}^e}{\partial E^e} \\ &\Rightarrow (l^e\mathbf{I} + \mathbf{k}_{\text{str}}^e)\left(\frac{\partial \mathbf{k}^e}{\partial E^e}\right) = l^e\frac{\partial \mathbf{k}_{\text{str}}^e}{\partial E^e} - \frac{\partial \mathbf{k}_{\text{str}}^e}{\partial E^e}\mathbf{k}^e \\ &\Rightarrow \frac{\partial \mathbf{k}^e}{\partial E^e} = \left(l^e\frac{\partial \mathbf{k}_{\text{str}}^e}{\partial E^e} - \frac{\partial \mathbf{k}_{\text{str}}^e}{\partial E^e}\mathbf{k}^e\right)(l^e\mathbf{I} + \mathbf{k}_{\text{str}}^e)^{-1} \end{aligned} \tag{39}$$

where

$$\mathbf{k}_{\text{str}}^e = E^e\int \mathbf{B}^{\mathrm{T}}\mathbf{DB}d\Omega^e \Rightarrow \frac{\partial \mathbf{k}_{\text{str}}^e}{\partial E^e} = \int \mathbf{B}^{\mathrm{T}}\mathbf{DB}d\Omega^e \tag{40}$$

Moreover, in Eq. (24), the required derivative of Young's modulus is calculated as follows:

$$\frac{\partial E^e}{\partial \sigma^e} = \frac{-E_0 m\beta(\sigma^e)^{m-1}}{\left(1 + \beta(\sigma^e)^m\right)^2} \tag{41}$$

and finally, the derivative of von Mises stress would be obtained

$$\frac{\partial \sigma^e}{\partial E^e} = \frac{\sigma^e}{E^e} \tag{42}$$

3.2 Sensitivity Verification With Finite Difference Method. Since sensitivity analysis is the core of the gradient-based optimization methods, it is critical to verify the accuracy of the presented adjoint method. To this end, the results from the obtained analytical relations are compared with the numerical results calculated by the finite difference method. The following forward finite difference equation is used for computing numerical derivative of stored strain energy (C) with respect to design variable x^e:

$$\frac{\Delta C}{\Delta x^e} \approx \frac{C(x^e + \Delta x^e) - C(x^e)}{\Delta x^e} \tag{43}$$

Table 1 Finite difference and analytical results

El. No.	Finite difference	Analytical	El. No.	Finite difference	Analytical
1	−2.011582012	−2.011585349	11	−0.563482416	−0.56345128
2	−1.05231166	−1.052320516	12	−0.742240402	−0.742199705
3	−1.063933297	−1.063959995	13	−0.326370042	−0.326420441
4	−2.031656265	−2.031705055	14	−0.348299167	−0.348309037
5	−1.170171871	−1.170160484	15	−0.409829681	−0.409815976
6	−0.807818168	−0.807900608	16	−0.298555491	−0.298533571
7	−0.820285351	−0.820357585	17	−0.053574922	−0.053574249
8	−1.189253496	−1.189197182	18	−0.447473525	−0.447516982
9	−0.692880064	−0.692903377	19	−1.052577048	−1.052589049
10	−0.527483479	−0.527478088	20	−2.179443825	−2.179498702

A perturbation value $\Delta x^e = 10^{-6}$ is used herein. A cantilever beam, which is shown in Fig. 6, is discretized by 20 elements. The adopted solid material properties are $E = 1\,\mathrm{N/m^2}$, $\nu = 0.3$, $m = 2$, and $\beta = 10$. The results for the finite difference and analytical are compared in Table 1. As it can be seen, a typical agreement up to four significant digits of precision is obtained which indicates the validity of the presented adjoint method.

3.3 Stability and Convergence. Stress relaxation due to the creep effect in TO causes some instabilities similar to stress constrained TO problems. This is because the value for the elasticity coefficient (E^e) depends on the stress value. In such problems and in both SIMP and ECP methods, it is needed to modify the stress calculation relation. To describe this problem, assume a simple plate under tension which is shown in Fig. 9(*a*). The optimum expected layout for the linear analysis ($\beta = 0$) and volfrac = 0.33 is depicted in Fig. 9(*b*). Here, Poisson's ratio is zero.

If the same problem is solved considering stress relaxation (for example, $m = 2$ and $\beta = 500$), the algorithm does not converge and it oscillates between two layouts which are shown in Fig. 10.

This problem occurs because the stress in low stiffened elements tends to zero instead of being infinite. The same problem would be seen in the stress-based TO using SIMP method. Assume we have just one element under force ($\mathbf{F}$) and the stiffness for all elements obtained by $\mathbf{k}_{\text{solid}} = \int_{\Omega_e} \mathbf{B}^{\mathrm{T}}\mathbf{D}\mathbf{B}d\Omega$. In the SIMP method and for element with density ρ, the displacement in nodal points is obtained from $\mathbf{u}^e = (\mathbf{k}_{\text{solid}}^{-1}\mathbf{F}/\rho^p E^e)$ and the stress tensor is calculated as follows:

$$\boldsymbol{\sigma} = \rho^q E^e \mathbf{B}\mathbf{D}\mathbf{u}^e = \rho^q E^e \mathbf{B}\mathbf{D}\frac{\mathbf{k}_{\text{solid}}^{-1}\mathbf{F}}{\rho^p E^e} = \rho^{q-p}\left(\mathbf{B}\mathbf{D}\mathbf{k}_{\text{solid}}^{-1}\mathbf{F}\right) \tag{44}$$

Therefore, the necessary condition of convergence in SIMP method is $q < p$ [41]. This condition guarantees that the stress tends to be infinite when density approaches zero. To overcome this problem in the I-ECP method, one might utilize the same idea of using different mapping relations for calculating the stiffness of links in stiffness matrix (l^e) and in computing stress in element ($l^{e\prime}$). Hence, the stress in the same problem of one element under force ($\mathbf{F}$) by I-ECP method is obtained as follows:

$$\begin{aligned}\boldsymbol{\sigma} &= E^e\mathbf{B}\mathbf{D}\mathbf{u}^{\text{in}} = E^e\mathbf{B}\mathbf{D}\left(l^{e\prime}\mathbf{I} + E^e\mathbf{k}_{\text{solid}}\right)^{-1} l^{e\prime}\mathbf{u}^{\text{out}} \\ &= E^e\mathbf{B}\mathbf{D}\left(l^{e\prime}\mathbf{I} + E^e\mathbf{k}_{\text{solid}}\right)^{-1} l^{e\prime}\left(\mathbf{k}_{\text{con}}^{-1}\mathbf{F}\right) \\ &= E^e\mathbf{B}\mathbf{D}\left(l^{e\prime}\mathbf{I} + E^e\mathbf{k}_{\text{solid}}\right)^{-1} l^{e\prime}\left(\frac{1}{E^e}\left(\mathbf{I} + \frac{1}{l^e}E^e\mathbf{k}_{\text{solid}}\right)\mathbf{k}_{\text{solid}}^{-1}\mathbf{F}\right) \\ &= \mathbf{B}\mathbf{D}\left(l^{e\prime}\mathbf{I} + E^e\mathbf{k}_{\text{solid}}\right)^{-1}\left(\left(l^{e\prime}\mathbf{I} + \frac{l^{e\prime}}{l^e}E^e\mathbf{k}_{\text{solid}}\right)\mathbf{k}_{\text{solid}}^{-1}\mathbf{F}\right)\end{aligned} \tag{45}$$

Here, we used

$$\begin{aligned}&\mathbf{k}_{\text{Con}}^e = \mathbf{k}_s^e\left(\mathbf{I} + \frac{1}{l^e}\mathbf{k}_s^e\right)^{-1} \Rightarrow \mathbf{k}_{\text{Con}}^e\left(\mathbf{I} + \frac{1}{l^e}\mathbf{k}_s^e\right) = E^e\mathbf{k}_{\text{solid}} \\ &\Rightarrow \mathbf{k}_{\text{Con}}^e\left(\mathbf{I} + \frac{1}{l^e}\mathbf{k}_s^e\right)\mathbf{k}_{\text{solid}}^{-1} = E^e\mathbf{I} \Rightarrow \mathbf{k}_{\text{Con}}^{-1} = \frac{1}{E^e}\left(\mathbf{I} + \frac{1}{l^e}\mathbf{k}_s^e\right)\mathbf{k}_{\text{solid}}^{-1}\end{aligned} \tag{46}$$

Therefore, the condition for the convergence is

$$\lim_{x\to 0}\left[\left(l^{e\prime}\mathbf{I} + E^e\mathbf{k}_{\text{solid}}\right)^{-1}\left(l^{e\prime}\mathbf{I} + \frac{l^{e\prime}}{l^e}E^e\mathbf{k}_{\text{solid}}\right)\mathbf{u}_{\text{soild}}^e\right] = \infty \tag{47}$$

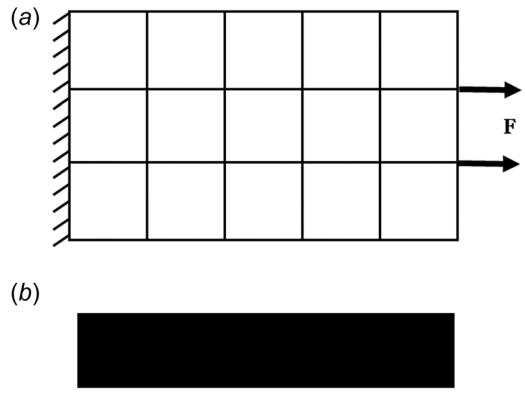

Fig. 9 (*a*) Simple plate with 15 elements and (*b*) the optimum layout for $\beta = 0$

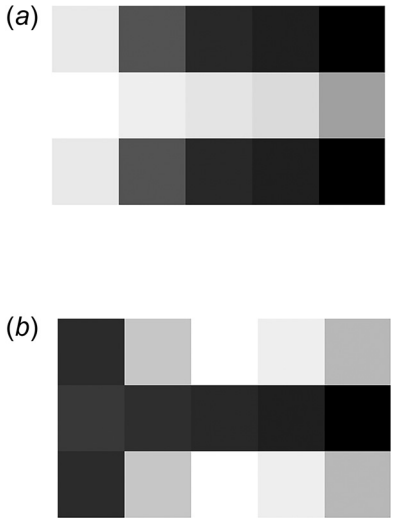

Fig. 10 Oscillating in the optimum layout for $\beta = 500$

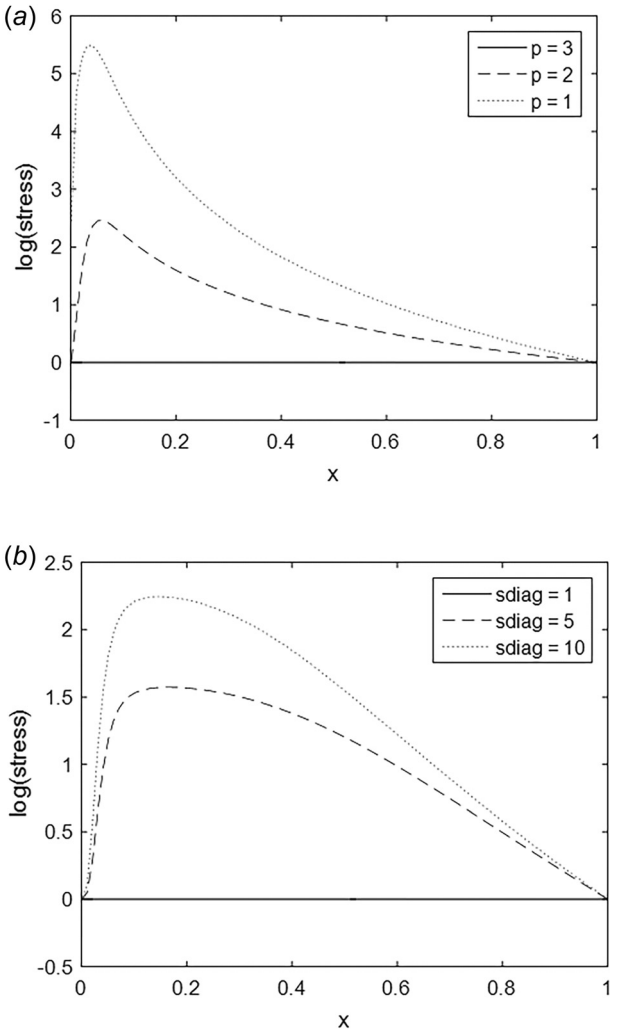

Fig. 11 The relation between stress and x^e using different (*a*) penalty and (*b*) *s*diag

Different mapping ($l^{e'}$) can be obtained by change in the parameter p or $s$diag used in Eq. (10). Figure 11 shows the effect of these parameters on the stress when design variable (x^e) approaches zero.

Therefore, change in the penalty power or $s$diag value does not work for solving the convergence problem because the obtained value for the stress is zero when x^e approaches zero. One idea is using the following relation to compute the stress:

$$\boldsymbol{\sigma}^e = \frac{1}{x^e} E^e \mathbf{B}\mathbf{u}^{\text{in}} \tag{48}$$

Figure 12(*a*) shows the efficiency of using Eq. (48) in calculating stress in low stiffness elements. Moreover, utilizing this equation in I-ECP method leads to desired optimum layout (Fig. 12(*b*)) for the problem defined in Fig. 9(*a*). It should be noted that since the value of design variable (x^e) for the element inside the domain (Ω) is one, then the stress in the final optimum layout is calculated correctly. This modification was implemented in the sensitivity analysis. Therefore, Eq. (25) should be modified as follows:

$$B^e_{s-1} = \frac{dE^e_{s-1}}{d\sigma^e_{s-1}} \times \frac{\partial \sigma^e_{s-1}}{\partial x^e} + \frac{dE^e_{s-1}}{d\sigma^e_{s-1}} \left(\frac{d\sigma^e_{s-1}}{d\mathbf{u}^{\text{in}}_{s-1}}\right)^{\text{T}} \times \left(\left(\mathbf{k}^e_I + \mathbf{k}^e_{s-2}\right)^{-1} \times \frac{dl^e}{dx} \left(\mathbf{u}^{\text{out}}_{s-1} - \mathbf{u}^{\text{in}}_{s-1}\right) \right) \tag{49}$$

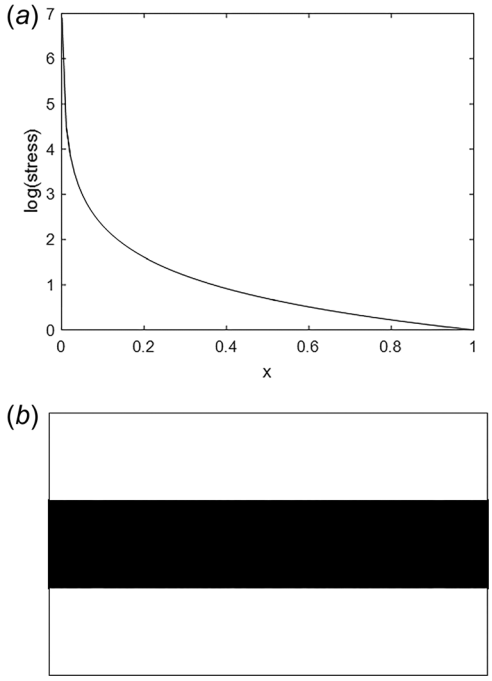

Fig. 12 (*a*) The relation between stress and x^e for $\sigma = (1/x^e)E^e\mathbf{B}\mathbf{u}^{\text{in}}$ and (*b*) the optimum layout for $\beta = 500$

where

$$\frac{\partial \sigma^e_{s-1}}{\partial x^e} = \frac{-1}{x^e} \sigma^e_{s-1} \tag{50}$$

Moreover, Eq. (38) would be

$$\frac{\partial \sigma_v}{\partial \mathbf{u}^{\text{in}}(i)} = \frac{1}{x^e} \left(\frac{E^e}{2\sigma_v}\right) \times \left((\mathbf{DB})_{1,i}(2\sigma_{11} - \sigma_{22}) + (\mathbf{DB})_{2,i}(2\sigma_{22} - \sigma_{11}) + 6(\mathbf{DB})_{3,i}\sigma_{12} \right) \tag{51}$$

4 Results

To investigate the effect of the creep on the optimum layout, several examples have been solved by the proposed method. Without loss of generality, the following material properties were chosen for Young's modulus and Poisson ratio: $E = 1\,\text{N/m}^2$ and $\nu = 0.33$. The mesh independency filter similar to SIMP method [42] with filter radius $r_{\min} = 1.5\times$ size of the element is applied for all examples. Moreover, $m = 2$ in Eq. (4) and the number of steps in nonlinear FE analysis (n) is 10.

4.1 Example 1. The first example is the classic cantilever beam illustrated in Fig. 6 where one end of the beam is fixed, while a unit load is applied at the middle of other end. The design domain was discretized into 100×50 elements and the mass limit was set to 50% of the total domain. The optimum designs for different values of β (Eq. (4)) are shown in Figs. 13(*a*), 13(*c*), and 13(*e*). As can be seen, the optimum layout under creep has more structural element. This topology is common in the optimum design of nonlinear structures. If we reanalyze the design obtained for linear case (Fig. 13(*a*)) under creep effect for $\beta = 200$ and $\beta = 300$, the strain energy would be 39.5924 J and 43.0395 J, while the strain energy in the obtained optimum layouts from the proposed method (Figs. 13(*b*) and 13(*c*)) is less and is equal to 38.0078 J and 41.4702 J, respectively. This proves the efficiency of the proposed method for considering stress relaxation effect. However, the difference is not significant since the difference

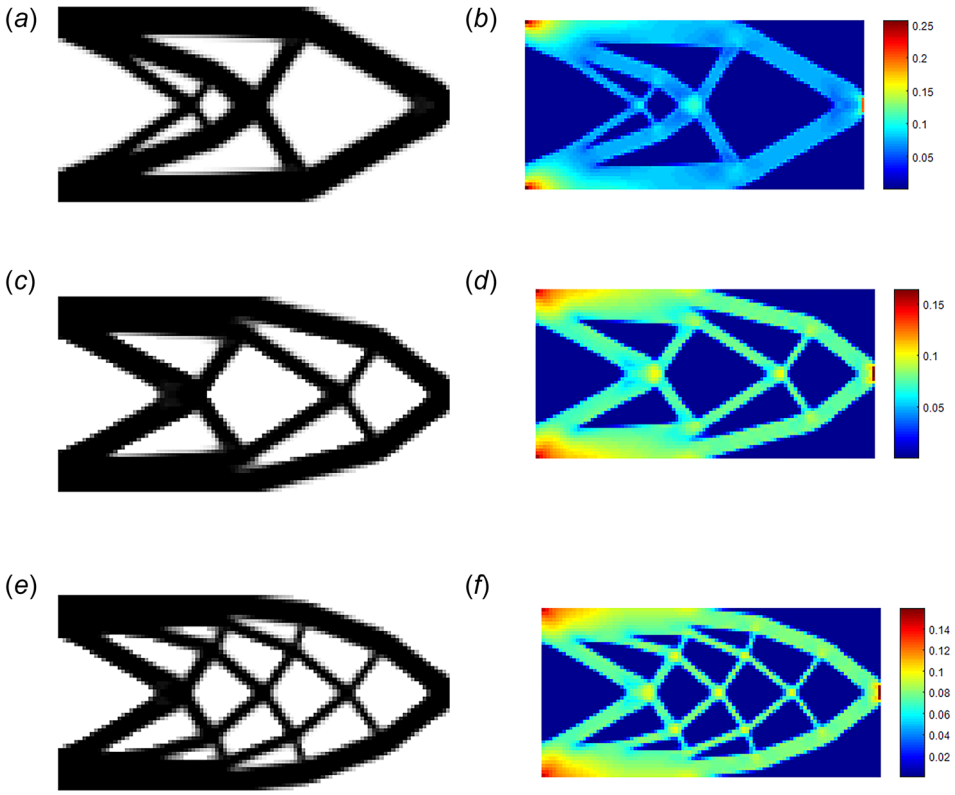

Fig. 13 Optimum layouts and stress distributions: (*a*) optimum layout for $\beta = 0$, $C = 31.9620$ J, (*b*) von Mises stress (N/m^2),$\sigma_{max} = 0.2563$ N/m^2, (*c*) optimum layout for $\beta = 200$, $C = 38.0078$ J, (*d*) von Mises stress (N/m^2), $\sigma_{max} = 0.1642$ N/m^2, (*e*) optimum layout for $\beta = 300$, $C = 41.4702$ J, and (*f*) von Mises stress (N/m^2), $\sigma_{max} = 0.1593$ N/m^2

Fig. 14 (*a*) Design domain and the boundary condition of beam example, (*b*) optimum layout for $\beta = 0$ ($C = 24.3057$ J), and (*c*) optimum layout for $\beta = 50$ ($C = 27.0388$ J)

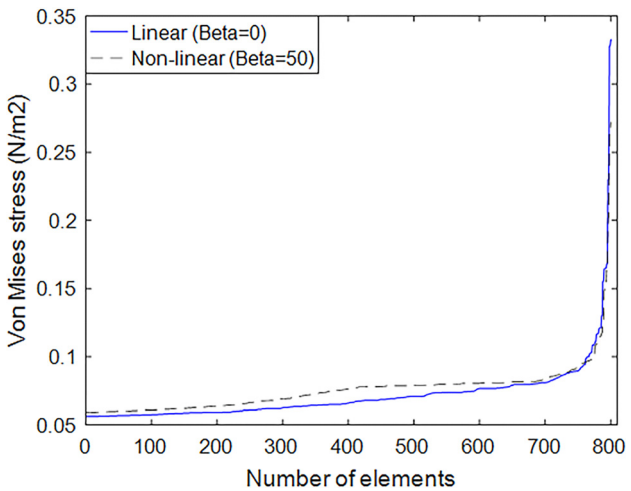

Fig. 15 Von Mises stress in high stress elements

between these layouts is not huge. Finally, the optimum layout should be chosen based on the material property and lifetime of the structure.

The von Mises stress fields in the optimum layouts are shown in Figs. 13(*b*), 13(*d*), and 13(*f*). By increasing the effect of creep (β), the stress field became more uniform and the value of the maximum stress reduced which was expected due to the stress relaxation.

4.2 Example 2. The second example is a simply supported beam from left and right sides and a unit concentrated load is applied at the top middle of the beam (Fig. 14(*a*)). The beam is discretized into 200×50 elements. Figures 14(*b*) and 14(*c*) depict

Fig. 16 Optimum layouts under $\beta = 50$ for the maximum displacement $u_{max} = 24.3$ (obtained volume $= 0.455 \times V_0$)

Fig. 17 (*a*) Design domain and the boundary condition for cantilever box shape, (*b*) optimum layout for $\beta = 0$ ($C = 1.7041$ J) and (*b*)$\beta = 50$($C = 1.7774$ J)

the optimum layouts with 40% mass constraint for linear case ($\beta = 0$) and under stress relaxation effect ($\beta = 50$). As expected, more structural element can be seen in the optimum layout considering stress relaxation. Reanalyzing the linear optimum layout under creep using $\beta = 50$ would give compliance equal to 29.8521 J. In comparison, the compliance for the obtained optimum design under creep is 27.0388 J which is less.

Von Mises stress in 800 high stress elements in both mentioned cases is sorted and plotted in Fig. 15. The maximum stress in the linear case is $0.3325\,\mathrm{N/m^2}$, while in domain under stress relaxation is $0.2720\,\mathrm{N/m^2}$. Moreover, under stress relaxation, the distribution of stress is more uniform as shown in Fig. 15.

The optimum layouts with the same value for the objective function ($C = 24.3$ J) are shown in Fig. 16. For the linear case, the volume of the optimum structure is 40% of the total design domain, while under stress relaxation ($\beta = 50$), the required volume for the optimum design is 45.4%. It means that if the maximum displacement during the lifetime of the structure is selected as constraint, the structure should be designed more conservatively with more mass.

4.3 Example 3. The design domain of the last example is shown in Fig. 17(*a*) which is discretized into 200×100 elements. The unit force is applied in the inclined direction at the center of the domain. Mass limit is selected as volfrac = 0.25. Figures 17(*b*) and 17(*c*) depict the optimum layout for linear and nonlinear cases.

In this example, the optimum layouts are almost the same in topology but there are differences in the shape of the obtained layouts. For example, the curvature and the thickness of the bars are different. This example is given to show that, in some cases, the stress relaxation causes difference just in the shape of layouts not in topology.

5 Conclusion

Creep as an important phenomenon in structures which experience high temperature leads to increment in the displacement field, and thus, it increases the nonlinear compliance (stored strain energy). However, due to the stress relaxation, the maximum stress in the structure is reduced. In this research, the effect of stress relaxation on the optimum layout of the structures was investigated. Topology optimization was performed by I-ECP method and stress relaxation is formulated in finite element analysis. Time-dependent adjoint method was used to calculate the required sensitivity in the optimization process.

Several benchmark problems are solved by the proposed method. The comparison between the strain energies in linear and nonlinear optimum layouts showed the efficiency of the proposed method. The obtained results stated that the optimum layouts under stress relaxation effect usually need more structural bars in compression with linear cases. However, the designs do not differ significantly. It would be expected to see more influences of the stress relaxation on the optimum layout, while stress is considered as a constraint or objective function in TO. Future work will focus on including stress relaxation effect in stress-constrained TO.

Acknowledgment

This work was supported by the National Research Foundation of Korea (NRF) (Global Frontier R & D Program on Center for Wave Energy Control based on Metamaterials).

Funding Data

- National Research Foundation of Korea (NRF) (Grant no. 2014M3A6B3063711) and MSIT (No. 2018R1A5A7025522).

References

[1] Doghri, I., 2013, *Mechanics of Deformable Solids: Linear, Nonlinear, Analytical and Computational Aspects*, Springer Science & Business Media, Berlin.
[2] Kawamoto, A., 2009, "Stabilization of Geometrically Nonlinear Topology Optimization by the Levenberg–Marquardt Method," Struct. Multidiscip. Optim., **37**(4), pp. 429–433.
[3] Bendsøe, M. P., and Kikuchi, N., 1988, "Generating Optimal Topologies in Structural Design Using a Homogenization Method," Comput. Methods Appl. Mech. Eng., **71**(2), pp. 197–224.
[4] Suzuki, K., and Kikuchi, N., 1991, "A Homogenization Method for Shape and Topology Optimization," Comput. Methods Appl. Mech. Eng., **93**(3), pp. 291–318.
[5] Swan, C. C., and Kosaka, I., 1997, "Voigt–Reuss Topology Optimization for Structures With Linear Elastic Material Behaviours," Int. J. Numer. Methods Eng., **40**(16), pp. 3033–3057.
[6] Bendsøe, M. P., 1989, "Optimal Shape Design as a Material Distribution Problem," Struct. Optim., **1**(4), pp. 193–202.
[7] Jung, D., and Gea, H. C., 2004, "Topology Optimization of Nonlinear Structures," Finite Elem. Anal. Des., **40**(11), pp. 1417–1427.
[8] Buhl, T., Pedersen, C. B., and Sigmund, O., 2000, "Stiffness Design of Geometrically Nonlinear Structures Using Topology Optimization," Struct. Multidiscip. Optim., **19**(2), pp. 93–104.
[9] Lee, H.-A., and Park, G.-J., 2012, "Topology Optimization for Structures With Nonlinear Behavior Using the Equivalent Static Loads Method," ASME J. Mech. Des., **134**(3), p. 031004.
[10] Bruns, T. E., and Tortorelli, D. A., 2003, "An Element Removal and Reintroduction Strategy for the Topology Optimization of Structures and Compliant Mechanisms," Int. J. Numer. Methods Eng., **57**(10), pp. 1413–1430.
[11] Huang, X., and Xie, Y., 2008, "Topology Optimization of Nonlinear Structures Under Displacement Loading," Eng. Struct., **30**(7), pp. 2057–2068.
[12] Ahmad, Z., Sultan, T., Zoppi, M., Abid, M., and Park, G. J., 2017, "Nonlinear Response Topology Optimization Using Equivalent Static Loads—Case Studies," Eng. Optim., **49**(2), pp. 252–268.
[13] Nakshatrala, P. B., Tortorelli, D. A., and Nakshatrala, K. B., 2013, "Nonlinear Structural Design Using Multiscale Topology Optimization—Part I: Static Formulation," Comput. Methods Appl. Mech. Eng., **261–262**, pp. 167–176.
[14] Xia, L., and Breitkopf, P., 2014, "A Reduced Multiscale Model for Nonlinear Structural Topology Optimization," Comput. Methods Appl. Mech. Eng., **280**, pp. 117–134.
[15] Xia, L., and Breitkopf, P., 2016, "Recent Advances on Topology Optimization of Multiscale Nonlinear Structures," Arch. Comput. Methods Eng., **2**(2), pp. 227–249.
[16] Luo, Q. T., and Tong, L. Y., 2016, "An Algorithm for Eradicating the Effects of Void Elements on Structural Topology Optimization for Nonlinear Compliance," Struct. Multidiscip. Optim., **53**(4), pp. 695–714.
[17] Zhang, X., Ramos, A. S., and Paulino, G. H., 2017, "Material Nonlinear Topology Optimization Using the Ground Structure Method With a Discrete Filtering Scheme," Struct. Multidiscip. Optim., **55**(6), pp. 2045–2072.
[18] Osher, S. J., and Santosa, F., 2001, "Level Set Methods for Optimization Problems Involving Geometry and Constraints—I: Frequencies of a Two-Density Inhomogeneous Drum," J. Comput. Phys., **171**(1), pp. 272–288.
[19] Allaire, G., Jouve, F., and Toader, A.-M., 2002, "A Level-Set Method for Shape Optimization," C. R. Math., **334**(12), pp. 1125–1130.
[20] Allaire, G., Jouve, F., and Toader, A.-M., 2004, "Structural Optimization Using Sensitivity Analysis and a Level-Set Method," J. Comput. Phys., **194**(1), pp. 363–393.

[21] Ha, S.-H., and Cho, S., 2008, "Level Set Based Topological Shape Optimization of Geometrically Nonlinear Structures Using Unstructured Mesh," Comput. Struct., **86**(13–14), pp. 1447–1455.
[22] Yoon, G. H., and Kim, Y. Y., 2005, "Element Connectivity Parameterization for Topology Optimization of Geometrically Nonlinear Structures," Int. J. Solids Struct., **42**(7), pp. 1983–2009.
[23] Yoon, G. H., and Kim, Y. Y., 2007, "Topology Optimization of Material-Nonlinear Continuum Structures by the Element Connectivity Parameterization," Int. J. Numer. Methods Eng., **69**(10), pp. 2196–2218.
[24] Yoon, G. H., and Kim, Y. Y., 2005, "The Element Connectivity Parameterization Formulation for the Topology Design Optimization of Multiphysics Systems," Int. J. Numer. Methods Eng., **64**(12), pp. 1649–1677.
[25] Langelaar, M., Yoon, G., Kim, Y., and Van Keulen, F., 2011, "Topology Optimization of Planar Shape Memory Alloy Thermal Actuators Using Element Connectivity Parameterization," Int. J. Numer. Methods Eng., **88**(9), pp. 817–840.
[26] Yoon, G. H., Kim, Y. Y., Langelaar, M., and van Keulen, F., 2008, "Theoretical Aspects of the Internal Element Connectivity Parameterization Approach for Topology Optimization," Int. J. Numer. Methods Eng., **76**(6), pp. 775–797.
[27] Yoon, G. H., Joung, Y. S., and Kim, Y. Y., 2007, "Optimal Layout Design of Three-Dimensional Geometrically Non-Linear Structures Using the Element Connectivity Parameterization Method," Int. J. Numer. Methods Eng., **69**(6), pp. 1278–1304.
[28] Yoon, G. H., 2010, "Maximizing the Fundamental Eigenfrequency of Geometrically Nonlinear Structures by Topology Optimization Based on Element Connectivity Parameterization," Comput. Struct., **88**(1–2), pp. 120–133.
[29] van Dijk, N. P., Yoon, G. H., van Keulen, F., and Langelaar, M., 2010, "A Level-Set Based Topology Optimization Using the Element Connectivity Parameterization Method," Struct. Multidiscip. Optim., **42**(2), pp. 269–282.
[30] Moon, S. J., and Yoon, G. H., 2013, "A Newly Developed qp-Relaxation Method for Element Connectivity Parameterization to Achieve Stress-Based Topology Optimization for Geometrically Nonlinear Structures," Comput. Methods Appl. Mech. Eng., **265**, pp. 226–241.
[31] Richard, B. H., and Eslami, M. R., 2008, *Thermal Stresses: Advanced Theory and Applications*, Springer, Dordrecht, The Netherlands.
[32] Betten, J., 2008, *Creep Mechanics*, Springer Science & Business Media, Berlin.
[33] Chen, W. J., and Liu, S. T., 2014, "Topology Optimization of Microstructures of Viscoelastic Damping Materials for a Prescribed Shear Modulus," Struct. Multidiscip. Optim., **50**(2), pp. 287–296.
[34] Amir, O., and Sigmund, O., 2013, "Reinforcement Layout Design for Concrete Structures Based on Continuum Damage and Truss Topology Optimization," Struct. Multidiscip. Optim., **47**(2), pp. 157–174.
[35] James, K. A., and Waisman, H., 2014, "Failure Mitigation in Optimal Topology Design Using a Coupled Nonlinear Continuum Damage Model," Comput. Methods Appl. Mech. Eng., **268**, pp. 614–631.
[36] James, K. A., and Waisman, H., 2015, "Topology Optimization of Viscoelastic Structures Using a Time-Dependent Adjoint Method," Comput. Methods Appl. Mech. Eng., **285**, pp. 166–187.
[37] Weertman, J., 1955, "Theory of Steady-State Creep Based on Dislocation Climb," J. Appl. Phys., **26**(10), pp. 1213–1217.
[38] Penny, R. K., and Marriott, D. L., 2012, *Design for Creep*, Chapman & Hall, Boca Raton, FL.
[39] Tegart, W. M., and Sherby, O. D., 1958, "Activation Energies for High Temperature Creep of Polycrystalline Zinc," Philos. Mag., **3**(35), pp. 1287–1296.
[40] Hayhurst, D., 1972, "Creep Rupture Under Multi-Axial States of Stress," J. Mech. Phys. Solids, **20**(6), pp. 381–382.
[41] Bruggi, M., 2008, "On an Alternative Approach to Stress Constraints Relaxation in Topology Optimization," Struct. Multidiscip. Optim., **36**(2), pp. 125–141.
[42] Sigmund, O., 2001, "A 99 Line Topology Optimization Code Written in Matlab," Struct. Multidiscip. Optim., **21**(2), pp. 120–127.